Oxidation of liquid gallium surface: Nonequilibrium growth kinetics in 2+1 dimensions

Y. L. Wang, Y. Y. Doong, T. S. Chen, and J. S. Haung
Institute of Atomic and Molecular Sciences, Academia Sinica, P.O. Box 23-166, Taipei, Taiwan
and Department of Physics, National Taiwan University, Taipei, Taiwan

(Received 7 October 1993; accepted 14 March 1994)

The formation process of a thin oxide film on liquid Ga is studied *in situ* using scanning ion microprobe imaging analysis. Oxide clusters form spontaneously on the liquid surface exposed to oxygen at room temperature. Small clusters diffuse and aggregate to form large clusters, and the process eventually leads to the formation of a thin porous oxide film. The fractal dimension of the oxide clusters is ~1.4. The total number of clusters in the system decays exponentially with time, while the average cluster size increases exponentially with time. These results are compared with Monte Carlo simulations based on different models of particle–particle and cluster–cluster aggregation.

I. INTRODUCTION

Oxidation of liquid metals is a subject that has been barely studied. Recently, researchers have successfully observed the oxidation process on a liquid metal Ga surface using secondary ion imaging microanalysis.[1] It was demonstrated that when Ga is exposed to oxygen at room temperature, oxidation does not proceed uniformly across the surface. Oxygen is adsorbed by the surface in the form of either oxygen or oxide, and these oxygen-containing particles diffuse and aggregate to form a thin porous oxide film. The fractal dimension[2] of this two-dimensional object is ~1.7, indicating the growth process is controlled by diffusion-limited aggregation (DLA) of the particles.[3]

Due to practical limitations, the previous oxidation experiments were conducted on a rather small liquid Ga surface area, $\leq(80\ \mu m)^2$. This sample area, or cleaned Ga "window", was created by locally removing the surface oxide, which forms naturally in air, using a Ga focused ion beam (FIB).[1,4] The unremoved oxide on the periphery of the window acts as a string of fixed nucleation sites for new oxide growth when the surface is exposed to O_2 at room temperature. There are several important issues that would be resolved if the size of the cleaned sample area could be made larger than the migration range of particles on the surface. On such a large sample area, the finite size effect caused by the artificial nucleation sites along the window periphery is eliminated and the observed oxidation should then approach that of an infinite system. Furthermore, it would help answer many questions about the oxidation process. For example, how does the initial oxide nucleation occur without the artificial oxide nucleation centers? And how does the oxidation proceed once the nucleation centers form spontaneously? We have successfully conducted oxidation experiments on a liquid Ga surface with a cleaned area as large as $(850\ \mu m)^2$, and found that the oxide growth pattern drastically deviated from the previous results on a small area. We report the experiment and compare the results with the theory of nonequilibrium particle aggregation kinetics.

II. EXPERIMENT

The experiment was conducted in a vacuum chamber (2×10^{-9} Torr base pressure) equipped with a focused ion beam (FIB) system (Fig. 1). The ion optics are a two-lens column (FEI company) with in-house modification for retarding field operation.[5,6] The beam energy can be varied from 100 eV to 25 keV. Throughout this experiment the beam energy was set at 25 keV. The ions are extracted from liquid Ga and focused to form a beam on the sample surface with an electronically variable diameter between 30 and 400 nm, and the corresponding beam currents are 6 pA and 6 nA, respectively. Two octopole scanners are employed to raster the beam across the sample. Secondary ions ejected by the FIB are detected with a channel electron multiplier overlooking the target area. The beam scanning, data acquisition, and image processing are achieved using a personal computer with in-house developed software. For secondary ion imaging analysis, the FIB is scanned across the sample with a fixed dwell time on each pixel element, and the number of pulses recorded by a channel electron multiplier during this time is translated into the gray level of the corresponding pixel of a picture. The images are stored digitally.

The liquid Ga sample was prepared by heating a piece of high purity (99.999%) Ga ingot on a stainless substrate to a temperature slightly above its melting point. The area and the thickness of the sample was about 1 cm^2 and 0.5 mm, respectively. Without appropriate seeding, Ga remains liquid at room temperature (25 °C) for an indefinite time. A layer of oxide, primarily Ga_2O_3,[7] forms naturally on its surface in air. Right before the sample was loaded into the load–lock system the oxide layer was scraped away, creating an optically brilliant surface. After the sample was loaded into the analysis chamber, the FIB was operated in the high current mode in order to locally clean the surface by sputtering. The size of the cleaned area ranged between $(850\ \mu m)^2$ and $(40\ \mu m)^2$, which also determined the ion beam current needed for the complete removal of the oxide. From the ion beam current and sputtering time, the thickness of the natural oxide film is estimated to be on the order of 10 nm, assuming the sputtering yield is 10.

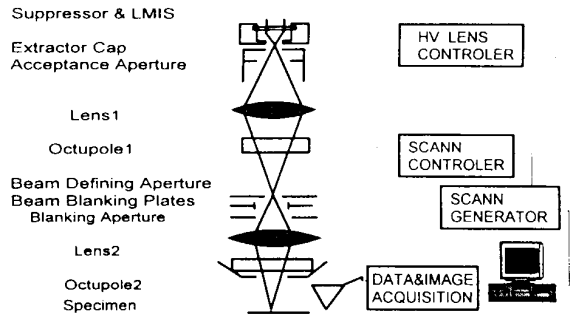

FIG. 1. Schematic of the scanning focused ion beam system.

The oxidation of the sample was achieved by backfilling the chamber with high purity (99.9999%) O_2 to a pressure between 5×10^{-7} and 1×10^{-6} Torr at room temperature. During the oxidation process, the FIB was blanked to avoid disturbing the growth. After the desired exposure was achieved, the O_2 was evacuated from the chamber and the FIB was operated in a low current (16 pA) mode to record the pattern of the oxide using secondary ion imaging analysis. Because of the destructive nature of the analysis, the low current operation was essential to avoid unnecessary disturbance of the film. Even with such a small beam current, the average beam current density is still ~1 μA/cm^2 for an examined area of (40 μm)^2. Experimentally, we found that high-current-density ion bombardment causes the oxide fragments in the vicinity of the beam to migrate into the beam. Such massive movement of oxide overlayer induced by ion beam bombardment was reported previously,[8] however, its mechanism remains to be understood.

For comparison, the pattern of the oxide grown on a (40 μm)^2 window after 200 L (1 L$=1\times10^{-6}$ Torr s) of O_2 exposure is shown in Fig. 2(a). The bright areas on the micrographs represent the location of the oxide, from where the secondary ion signal is ~5 times higher than that from cleaned Ga. This effect of oxygen enhancement of the secondary ion yield is well documented,[9] and it has been previously demonstrated for this particular material system using secondary ion mass spectrometery.[1,4] The pattern resembles a collection of DLA originating from the edge of the window where the unremoved oxide remains. Its fractal dimension is ~1.7, and the fourfold symmetry of the pattern is a result of the artificial arrangement of the nucleation centers. Figure 2(b) shows the oxide pattern grown on a (560 μm)^2 cleaned Ga area after 50 L of O_2 exposure. This dose of O_2 produces sparse oxide clusters covering $\sim10\%$ of the surface area. Figure 2(c) shows the same oxide clusters at a higher magnification (170 μm)^2. The pattern of the clusters is very different from that of DLA, and the average spacing between clusters is approximately 50 μm. This distance is consistent with the fact that isolated oxide islands were rarely observed in previous experiments conducted on small area [Fig. 2(a), and Refs. 1 and 4]. Apparently, the mean-free distance of the aggregating particles on the liquid surface is also ~50 μm. These particles have little chance to encounter each other and

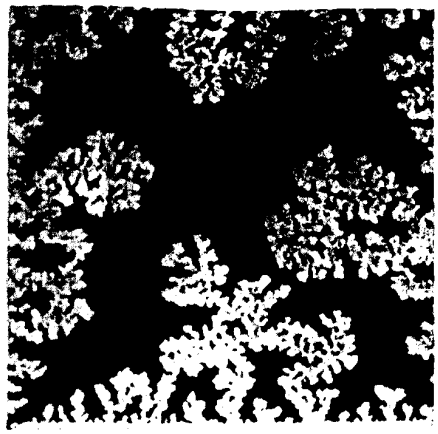

(a)

(b)

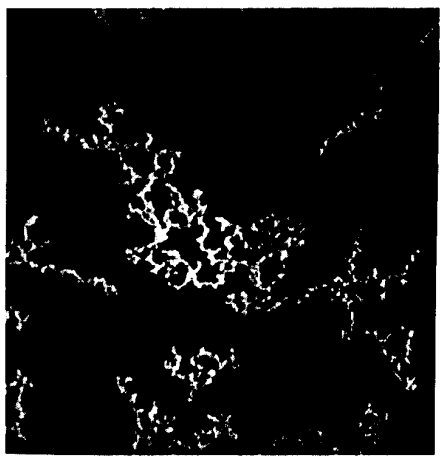

(c)

FIG. 2. Oxide patterns grown on cleaned liquid Ga "window" (see text) of different size (w) and for various O_2 exposure (J), at ~10 min after the exposure. (a) $w=40$ μm, $J=200$ L, f.s. (full scale)$=40$ μm; (b) $w=560$ μm, $J=100$ L, f.s.$=560$ μm; (c) $w=560$ μm, $J=100$ L, f.s.$=170$ μm.

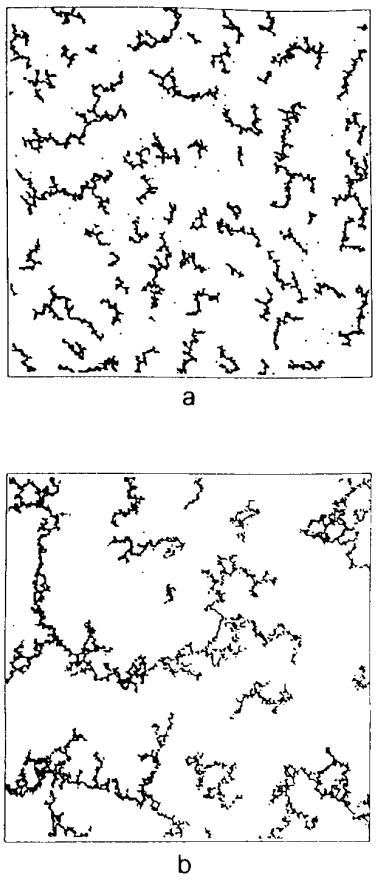

FIG. 3. Binary maps of oxide clusters grown on Ga surface at different time (t) after O_2 exposure (J). (a) $t=3$ min, $w=850$ μm, $J=50$ L, f.s.$=170$ μm, (b) $t=60$ min, $w=850$ μm, $J=50$ L, f.s.$=170$ μm.

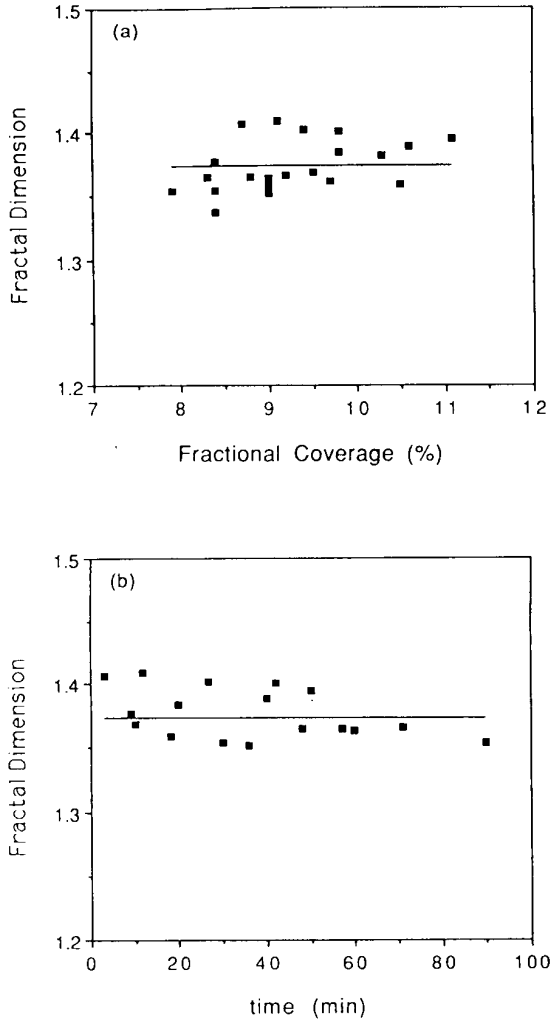

FIG. 4. Fractal dimensions D_f of the oxide cluster patterns as a function of the (a) fractional surface oxide coverage and (b) time after O_2 exposure. The straight line shows the average value of D_f.

form larger oxide clusters if they are confined to an area as small as $(80\ \mu m)^2$, the size of the area for the previous experiments. The only destiny for the particles is to aggregate to the unremoved oxide on the boundary. Based on this observation of the particle migration range (10–100 μm) and typical time (~100 s) required for the pattern formation, we estimate the diffusion coefficient of the aggregating particles is between 10^{-6} and 10^{-8} cm^2/s.

In order to gather quantitative information from the observed oxide pattern, the secondary ion images, with typical 256×256 pixels, are transformed into two-dimensional binary maps using a simple high-pass filter. Figure 3(a) shows a map $(170\ \mu m)^2$, taken from the center of a $(850\ \mu m)^2$ cleaned area, 3 min after 50 L of O_2 exposure. Note the contrast has been reversed for clarity. Figure 3(b) shows the oxide pattern 60 min later. Cluster to cluster aggregation is clearly observed. The fractal dimension (D_f) of the growth patterns are determined using the standard box counting methods.[10] Figure 4(a) shows the results taken for various fractional oxide coverage, and Fig. 4(b) at different times after O_2 exposure. D_f is 1.38 ± 0.03, and it is independent of time and fractional surface oxide coverage within the experimental uncertainty. D_f may have a small dependence on time. It however, is too small to draw any conclusion. These measurements also demonstrate the insensitivity of D_f to the cluster formation process. In other words, fractal dimension is almost invariant during the process of cluster–cluster aggregation.

The measured fractal dimension of the oxide clusters is essentially the same (~1.4) as that derived from models based on Monte Carlo simulation of the aggregation of rigid random clusters.[11,12] It is, therefore, interesting to try to understand the oxide cluster aggregation process within the theoretical framework of nonequilibrium cluster–cluster aggregation kinetics.[13–16] The most important observations derived from these simulations of diffusion-limited cluster–cluster aggregation (DLCCA) and reaction-limited cluster–cluster aggregation (RLCCA) are as follows. For DLCCA, the total number of clusters in the system $N(t)$ scales as

$$N(t) \propto t^{-z}, \tag{1}$$

while the time dependence of the mean cluster size $S(t)$ scales as

$$S(t) \propto t^{z}, \tag{2}$$

where z is a positive dynamical exponent and $S(t)$ is defined as

$$S(t) = \frac{\Sigma s^2 n_s(t)}{\Sigma s n_s(t)}, \tag{3}$$

The $n_s(t)$ in Eq. (3) is the number of clusters of size s at time t. For RLCCA, however, temporal scaling of $S(t)$ cannot be unambiguously derived from the results of the simulation. It can either scale as Eq. (2) with a large exponent or grow exponentially with time. Or it can even vary as

$$S(t) \propto (t - t_g)^{-\omega}, \tag{4}$$

where t_g is the gel time (i.e., the time it takes for all the clusters in a system to aggregate into a single cluster) and ω is another positive exponent. Neither can power law scaling of $N(t)$ be established from the simulations.[14] Figures 5(a), 6(a), and 5(b), 6(b) show the time dependence of $N(t)$ and $S(t)$ in semilogarithmic and logarithmic format, respectively. Although the data are somewhat scattered and definitive conclusions cannot be drawn, but exponential decay of $N(t)$ seems to be favored. If this is the case, then the reaction of oxide cluster–cluster aggregation is most likely limited by the rate of the chemical reaction which forms the bonds between the clusters, and not by the diffusion of the clusters.

III. DISCUSSION

The fact that spontaneous oxide nucleation clusters were not observed in previous studies on small Ga surfaces but they do appear on large area experiments has some interesting implications on the nature of the aggregating particles on the liquid surface. As stated before, these oxygen-containing particles could be in the form of adsorbed O_2 or oxide. Both types of particles could diffuse along the surface and aggregate to the boundary of the window, creating DLA-like oxide patterns. If we assume the diffusion of the adsorbed O_2 are responsible for the observed oxide pattern, and that there is a probability for them to form spontaneous nucleation centers, we can simulate this growth process by a Monte Carlo method, and check if the resulting aggregation pattern is consistent with the experimental observation.

By assuming that the diffusion of the adsorbed O_2 are responsible for the DLA-like oxide growth, we imply that oxide nuclei have a much smaller mobility than O_2. As a first approximation, we simply assume the oxide nuclei remain fixed in space once they are formed on the surface. Based on these simplifying assumptions, we design the following algorithm for simulating the growth process. A particle is landed randomly on a 256×256 square lattice, and starts its journey of random walk. For each step of walk, it has a probability S to permanently occupy its final position. If a particle makes contact with an occupied site, it automatically occupies its final position, similar to the DLA growth rule. A periodic boundary condition is used for all the simulations. In other words, when a particle wanders off the lattice, it comes back to the opposite side of the lattice. The results of the simulation for various S at a surface coverage of 25% are shown in Fig. 7. For $S=1$ [Fig. 7(a)], random distributions

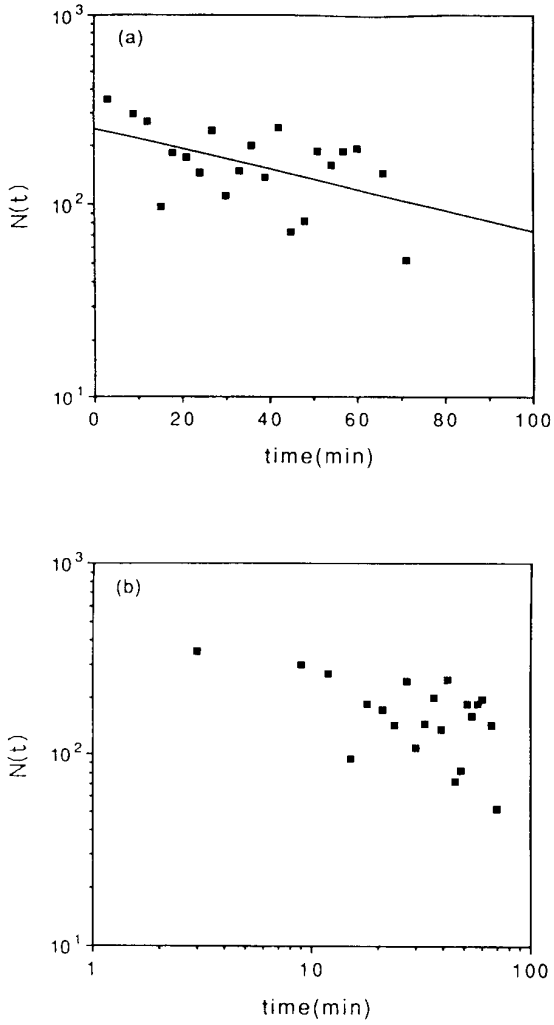

FIG. 5. Time dependence of the number of clusters in an area of (170 μm)^2. Data are plotted in (a) semilogarithmic and (b) logarithmic scale. The straight line in (a) shows the exponential fit to the data.

without any long-range correction appear as expected. As S is reduced [Figs. 7(b) and 7(c)], more and more clustering takes place, and the size of the clusters also grows correspondingly. For $S=10^{-6}$, the overall growth pattern resembles that of a collection of randomly distributed DLA. However, there are two factors that cause the individual clusters to deviate from DLA-like. First, the screening effect of DLA is suppressed because the particles are launched from the third dimension, and their access to the interior of the cluster is not blockaded. The effect caused by the growth interference among the clusters leads to a well-defined intercluster empty zone. By comparing Fig. 7(d) with Figs. 2(b) and 2(c), one readily comes to the conclusion that the oxide clusters are much more stringy, i.e., less branching occurs on these dendritic structures. The results of the simulation indicate the oxide cluster pattern is not just the result of DLA with spontaneous nucleation. We, therefore, believe that the particle responsible for the observed oxide clusters most likely is not in the form of adsorbed O_2. We postulate that

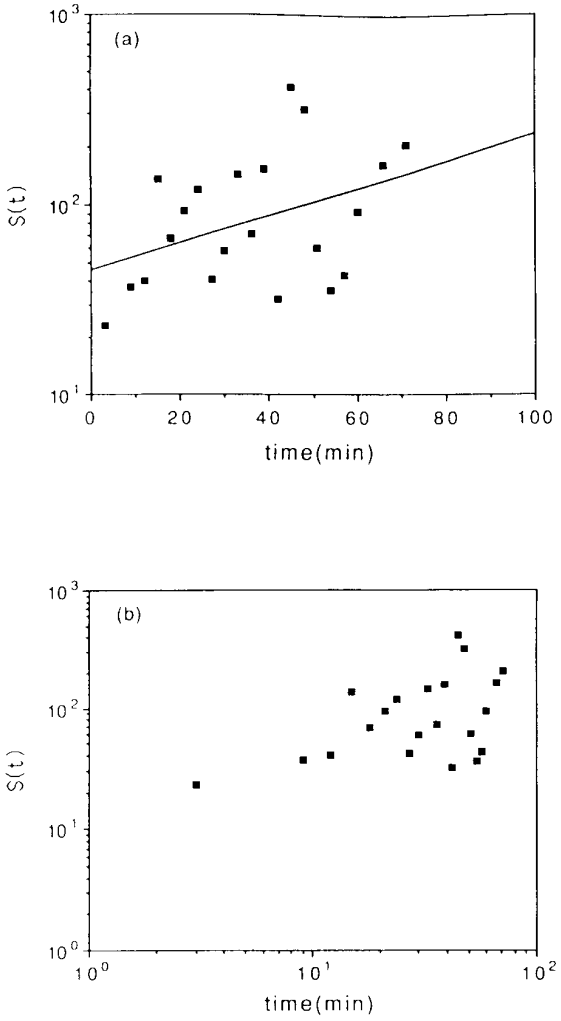

FIG. 6. Time dependence of the average size (see text) of the clusters in an area of (170 μm)^2. Data are plotted in (a) semilogarithmic and (b) logarithmic scale. The straight line in (a) shows the exponential fit to the data.

small oxide clusters, whose size is smaller than the detection limit of our experimental method (~100 nm), form on the Ga surface when exposed to O_2. If preexisting massive clusters are present within the migration range of the small clusters, they have little chance to aggregate among themselves and form larger clusters detectable by our method. Most of them simply diffuse on the surface and eventually form a collection of DLA-like patterns along the window edge as shown in Fig. 2(a). When the size of the window is made larger than the mean free distance of the small clusters, which is measured to be ~50 μm in this experiment, cluster–cluster aggregation becomes the favored growth mechanism.

In conclusion, we have studied the growth kinetics of the oxide film formation on the surface of liquid Ga. We found that random clusters of oxide form spontaneously on Ga when exposed to O_2 at room temperature. These clusters diffuse on the surface and aggregate to form larger clusters. By analyzing the fractal dimension, number of clusters, and average cluster size of the growth pattern, and comparing that with the results from Monte Carlo simulations, we believe that growth kinetics are dominated by reaction limited cluster–cluster aggregation. Experimentally, we have observed the deformation and relaxation of the clusters. These effects are not included in the existing simulation models. More experiments and simulations are needed for a better understanding of the growth process.

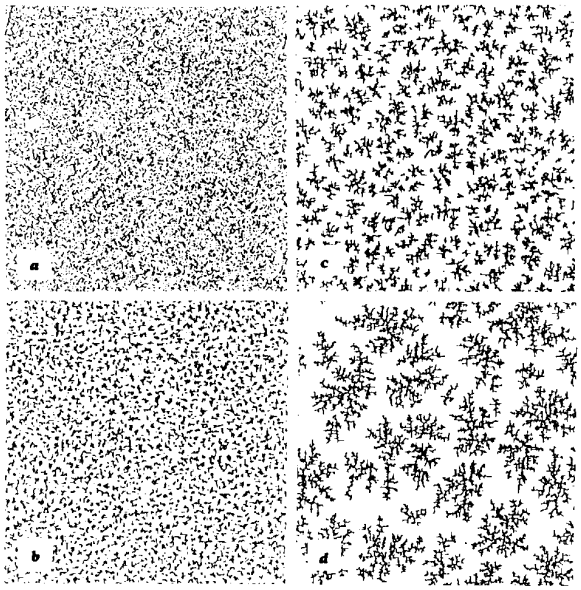

FIG. 7. Results of a simulation based on a model in which the diffusing particles have a finite spontaneous sticking probability S at each step of its random walk. (a) $S=1$, (b) $S=10^{-2}$, (c) $S=10^{-4}$, and (d) $S=10^{-6}$.

ACKNOWLEDGMENTS

The authors would like to acknowledge Dr. J. C. Lin, Dr. K. J. Song, M. Y. Lai, M. C. Yeng, and C. I. Wang for their suggestions and assistance. Professor R. Levi-Setti is acknowledged for providing the Ga sample. This work is partly supported by a grant from the National Science Council (Contract No. 82-0417-E-001-020), Taiwan, Republic of China.

[1] Y. L. Wang, A. Raval, and R. Levi-Setti, Scanning Microsc. **3**, 731 (1989).
[2] B. B. Mandelbrot, *Fractal Geometry of Nature* (Freeman, San Francisco, 1982).
[3] T. A. Witten and L. M. Sander, Phys. Rev. Lett. **47**, 1400 (1981).
[4] J. M. Chabala, Phys. Rev. B **46**, 11346 (1992).
[5] Y. L. Wang and Z. Shao, in *Advances in Electronics and Electron Physics*, edited by P. W. Hawkes (Academic, Boston, 1991), Vol. 81, pp. 177–209.
[6] Y. L. Wang, M. Y. Lai, and Z. Shao, J. Vac. Sci. Technol. A **11**, 406 (1993).
[7] C. Y. Su, P. R. Skeath, I. Lindau, and W. E. Spicer, Surf. Sci. **118**, 248 (1982).
[8] J. Fine, S. C. Hardy, and T. D. Andreadis, J. Vac. Sci. Technol. **18**, 1310 (1981).
[9] A. Benninghoven, F. G. Rudenauer, and H. W. Werner, *Secondary Ion Mass Spectrometry* (Wiley, New York, 1987).

[10]M. Schroeder, *Fractals, Chaos Power Laws* (W. H. Freeman, New York, 1991), p. 213.
[11]P. Meakin, Phys. Rev. Lett. **51**, 1119 (1983).
[12]M. Kolb, R. Botet, and R. Jullien, Phys. Rev. Lett. **51**, 1123 (1983).
[13]T. Vicsek and F. Family, Phys. Rev. Lett. **51**, 1123 (1983).
[14]P. Meakin and F. Family, Phys. Rev. A **38**, 2110 (1988).
[15]D. J. Robinson and J. C. Earnshaw, Phys. Rev. A **38**, 2055 (1992).
[16]D. J. Robinson and J. C. Earnshaw, Phys. Rev. Lett. **71**, 715 (1993).